PHYSICAL REVIEW B **79**, 180301(R) (2009)

Localization-delocalization transition of a polaron near an impurity

A. S. Mishchenko,[1,2] N. Nagaosa,[1,3] A. Alvermann,[4] H. Fehske,[4] G. De Filippis,[5] V. Cataudella,[5] and O. P. Sushkov[6]
[1]*Cross-Correlated Materials Research Group (CMRG), ASI, RIKEN, Wako 351-0198, Japan*
[2]*RRC "Kurchatov Institute," 123182 Moscow, Russia*
[3]*Department of Applied Physics, The University of Tokyo, 7-3-1 Hongo, Bunkyo-ku, Tokyo 113, Japan*
[4]*Institut für Physik, Ernst-Moritz-Arndt-Universität Greifswald, 17489 Greifswald, Germany*
[5]*Dip. di Scienze Fisiche and Coherentia-CNR-INFM, Università di Napoli Federico II, I-80126 Napoli, Italy*
[6]*School of Physics, University of New South Wales, Sydney, New South Wales 2052, Australia*
(Received 9 March 2009; published 11 May 2009)

We solve the problem of polaron localization on an attractive impurity by means of direct-space diagrammatic Monte Carlo implemented for the system in the thermodynamic limit. In particular we determine the ground-state phase diagram in dependence on the electron-phonon coupling and impurity potential strength for the whole phonon frequency range. Including the quantum phonon effects we find and characterize a phase where self-trapped polarons are not localized at shallow impurities, which is missing in the adiabatic approximation. We show that near the localization transition a region with a mixture of weak- and strong-coupling spectral responses is realized.

DOI: 10.1103/PhysRevB.79.180301 PACS number(s): 71.10.Fd, 02.70.Ss, 71.38.−k

A general approach to the theoretical description of a particle in a bulk medium coupled to both bosonic excitations and potential of imperfections is an important but notoriously hard problem that poses a real challenge even to modern nonperturbative approaches.[1] As yet only approximate results, relying, e.g., on dynamical-mean field theory exist. A central question in this context is the formation of three-dimensional (3D) polarons at impurities, or the Anderson localization of polarons in disordered media.[2–4] The overall importance of the physics of electron-phonon interaction in doped materials makes this issue of general interest for different areas of physics and technology. As a matter of fact the interplay between disorder and interaction effects is an important issue for contemporary materials design. For example, high-T_c superconductors[5–7] or materials with colossal magnetoresistance[8] are doped Mott insulators where besides the coupling to bosonic excitations (phonons and magnons) disorder is present.

In this Rapid Communication we present the numerically exact solution to the polaron problem in the presence of an attractive impurity in a 3D material. The accepted model for that situation is given by the Hamiltonian $H=H^{(0)}+H^{(1)}$ with

$$H^{(0)} = -Uc_{\mathbf{0}}^{\dagger}c_{\mathbf{0}} + \omega_{\mathrm{ph}}\sum_{\mathbf{i}} b_{\mathbf{i}}^{\dagger}b_{\mathbf{i}}, , \tag{1}$$

$$H^{(1)} = -t\sum_{\langle \mathbf{i},\mathbf{j}\rangle} c_{\mathbf{i}}^{\dagger}c_{\mathbf{j}} - \gamma\sum_{i}(b_{\mathbf{i}}^{\dagger}+b_{\mathbf{i}})c_{\mathbf{i}}^{\dagger}c_{\mathbf{i}}. \tag{2}$$

In $H^{(0)}$, U is the attractive impurity potential for the electron $c_0^{\dagger}$ at site 0 and $b_i^{\dagger}$ creates a dispersionless optical phonon with frequency ω_{ph} at Wannier site i. $H^{(1)}$ describes the electron transfer $\propto t$ between nearest-neighbor sites and local Holstein coupling to the phonons $\propto\gamma$.

In the absence of electron-phonon (el-ph) coupling ($\gamma=0$), the critical U for particle localization at the impurity is $U_c(\gamma=0)\approx 3.96$ (Ref. 9) (all energies, potentials, and frequencies are measured in units of t) which equals $\varepsilon(1)$ in Ref. 9 and is 1/12 of the bandwidth W_B in Ref. 10. In the adiabatic approximation (AA) $\omega_{\mathrm{ph}}=0$, the phase diagram in U-λ coordinates was established in Ref. 10 [our dimensionless coupling constant $\lambda=\gamma^2/(6t\omega_{\mathrm{ph}})$ is equal to their g]. The phase boundary in AA, separating delocalized polaron states from localized ones, crosses the U axis at $U_c(\gamma=0)$ and the λ axis at $\lambda_c(U_c=0,\ \omega_{\mathrm{ph}}=0)\approx 0.9$. The latter crossing is a confusing property of the AA phase diagram since it implies that for el-ph couplings $\lambda>\lambda_c(U_c=0,\ \omega_{\mathrm{ph}}=0)$ the polaron is localized even when $U=0$. Quite the contrary, a particle is never localized in a translationally invariant lattice ($U=0$) with quantum phonons ($\omega_{\mathrm{ph}}>0$). Instead the particle undergoes only a crossover from the weak-coupling light polaron to a strong-coupling heavy polaron with small radius around a self-trapping coupling λ_{ST}.[11] The AA erroneously equates λ_{ST} with the critical el-ph coupling strength λ_c required for polaron localization at $U\neq 0$. Therefore drastic differences between the approximation-free result and that obtained in AA are expected, especially at small U_c.

Having this delicate situation in mind, we decided to study the full Hamiltonian [Eqs. (1) and (2)] with quantum phonons. To this end we employ a scheme combining the diagrammatic Monte Carlo (DMC) method in direct space[12] and the stochastic optimization method for analytic continuation[12,13] which provides the approximation-free solution of the above problem without finite-size errors and for zero temperature ($T=0$). Calculating the charge density distribution (CDD) around the impurity and the local density of states (LDOS) on the impurity site, we establish the localization phase diagram for different phonon frequencies. We characterize two polaronic regimes in a system with impurities. The polaron at small U can be self-trapped though extended and not yet confined by shallow impurities. The other regime, arising near the critical parameters for localization at the impurity, shows spectroscopic response such as a mixture of spectra typical for weak, intermediate, and strong couplings.

Note that the present model is valid only for electronic impurities such as those in high-T_c superconductors[5–7] or

materials with colossal magnetoresistance.[8] For lattice impurities, such as vacancies, one has to take into account local phonon modes with different frequencies ($\neq\omega_{\mathrm{ph}}$). The corresponding modification of the localization diagram is beyond the present study but can be treated by the DMC method suggested here as well.

The direct-space DMC method[14] can provide the direct-space Green's functions (GFs) in imaginary time (τ) representation at $T=0$ $G_{\mathbf{ij}}(\tau)=\langle \mathrm{vac}|c_{\mathbf{j}}(\tau)c_{\mathbf{i}}^{\dagger}|\mathrm{vac}\rangle$ for the Hamiltonian [Eqs. (1) and (2)] by Feynman diagram expansion in the interaction representation,

$$G_{\mathbf{ij}}(\tau)=\left\langle e^{-\tau H^{(0)}}\hat{T}_{\tau}\left[c_{\mathbf{j}}(\tau)c_{\mathbf{i}}^{\dagger}\exp\left\{-\int_{0}^{\tau}H^{(1)}(\tau')d\tau'\right\}\right]\right\rangle. \tag{3}$$

The implementation of DMC (Ref. 14) requires keeping in computer memory all GFs $\{G_{\mathbf{ij}}(\tau)\}$ in direct space, which restricts the lattice to about 25×25 sites. To avoid this size limitation we calculate only quantities related to on-site GFs $G_{\mathbf{ii}}(\tau)$. We are able to calculate the on-site GFs at $T=0$ for a $10^8\times10^8\times10^8$ lattice, thereby avoiding any finite-size or finite T errors. A slight modification of Eq. (3),

$$n(\mathbf{i})=\left\langle \frac{e^{-\beta H^{(0)}}}{Z}\hat{T}_{\tau}\left[c_{\mathbf{i}}(\beta)c_{\mathbf{i}}^{\dagger}\exp\left\{-\int_{0}^{\beta}H^{(1)}(\tau')d\tau'\right\}\right]\right\rangle, \tag{4}$$

introduces the estimator for the CDD at $T=\beta^{-1}$. To make a calculation of the CDD feasible, we collect its statistics in a cube with 40^3 number of sites. Note that this strategy does not introduce finite-size errors because only the $\tau=0,\beta$ points of the partition function loop are confined to the 40^3 cube while the diagrams are free to sample all $(10^8)^3$ sites. Hence, this is the only method that can deal with long-range impurity potentials, say, of Coulomb type.

The CDD estimator is effective for locating the localization parameters for large U only but, since it requires finite T, fails at small $U\ll t$. Note that the path-integral quantum Monte Carlo algorithm,[15] which is another method relevant for the present problem, requires careful control of precision for the same reason. As it is shown by comparison with our data, such control can be successfully performed.[4] However, the most rigorous method to locate the localization point in the infinite system is to calculate the on-site $T=0$ GF $G_{\mathbf{ii}}(\tau)$, determine the LDOS $L_{\mathbf{i}}(\omega)=-\pi^{-1}\,\mathrm{Im}\,G_{\mathbf{ii}}(\omega)$ by analytic continuation,[12,13] and check for the presence of a bound state in the LDOS $L_0(\omega)$ at the impurity site. Although not yet applied, the variational method[16] also has obvious potential to solve the current problem.

To validate the implementation of the DMC technique, we located the critical $U_c(\lambda=0)\approx3.96$ by calculating the CDD, normalized to unity at the impurity site, around the impurity. It occurred that for $U\leq U_c$ the charge density does not decrease exponentially with distance from the impurity while for $U>U_c$ it does. Perfect agreement is found between CDD obtained by DMC and that obtained in Ref. 9. For U close to U_c, however, determination of the LDOS $L_{\mathbf{0}}(\omega)$ is a much more precise method since the CDD requires finite T.

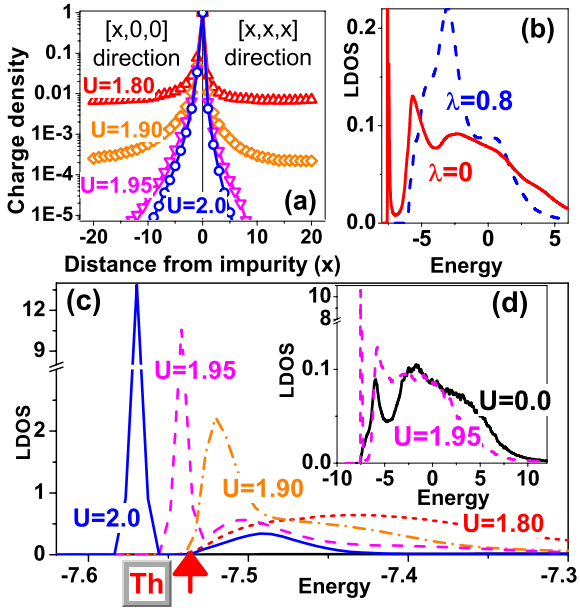

FIG. 1. (Color online) Charge density (normalized to unity at the impurity site) at $T=0.001$ along the (a) [1,0,0] and [1,1,1] directions and LDOS at the impurity site for [(c) and (d)] $T=0$ for different values of U at $\omega_{\mathrm{ph}}=2$ and $\lambda=0.8$. The arrow in panel (c) indicates the lower threshold (Th) of the spectrum at $\lambda=0.8$ and $U=0$. Panel (b) shows LDOS at the impurity site at $U=2$ and $\omega_{\mathrm{ph}}=2$ for $\lambda=0$ (dashed line) and $\lambda=0.8$ (solid line). Error bars in panel (a) are smaller than 10^{-5} (much less than point size).

First let us demonstrate how trapped polaron states are determined using the LDOS. From the commutator $[H,c_i^{\dagger}]$ we find that, independent of the el-ph coupling λ, the first moment M_1 of the LDOS $L_{\mathbf{i}}(\omega)$ obeys $M_1=\int_{-\infty}^{\infty}d\omega\ \omega L_{\mathbf{i}}(\omega)=-U\delta_{\mathbf{i},\mathbf{0}}$. In accordance with this sum rule, the LDOS at the impurity site shifts to lower energies with increasing U [Fig. 1(c)]. The second moment $M_2=\int_{-\infty}^{\infty}d\omega\ \omega^2L_{\mathbf{i}}(\omega)$ increases with λ [Fig. 1(b)], and the overall LDOS broadens. Figure 1 shows the (a) CDD and [(c) and (d)] LDOS as a function of U. Let us start the discussion with the case $U=0$, where no localization is expected. We determine the lower border $E_{\mathrm{Th}}(\lambda)$ of the LDOS $L_0(\omega)$ for given λ [arrow in Fig. 1(c)]. Increasing U the LDOS changes but there is no spectral density below $E_{\mathrm{Th}}(\lambda)$ up to $U\leq1.90$ [Fig. 1(c)]. The CDD around the impurity, in accordance with the absence of a bound state in LDOS, does not show exponential decrease as well [Fig. 1(a)]. This gives another confirmation for the method employed here. In order to search for the localization-delocalization transition we proceed to larger values of U. For $U\geq1.95$, the bound state appears below the threshold $E_{\mathrm{Th}}(\lambda)$ [Fig. 1(c)], and the CDD decays exponentially [Fig. 1(a)]. In this way we obtain one transition point in the phase diagram [Fig. 2(a)], here $U_c(\omega_{\mathrm{ph}}=2,\ \lambda=0.8)=1.925\pm0.025$. Recall that, although the LDOS approach needs a very precise calculation [compare Figs. 1(c) and 1(d)], it is applicable for any values of λ and U. On the contrary, the CDD method is fast but, due to requirement of finite T, not reliable at $U\ll1$.

Next the phase diagram for polaron localization is presented in Fig. 2. Using λ_c-U_c coordinates [Figs. 2(a) and

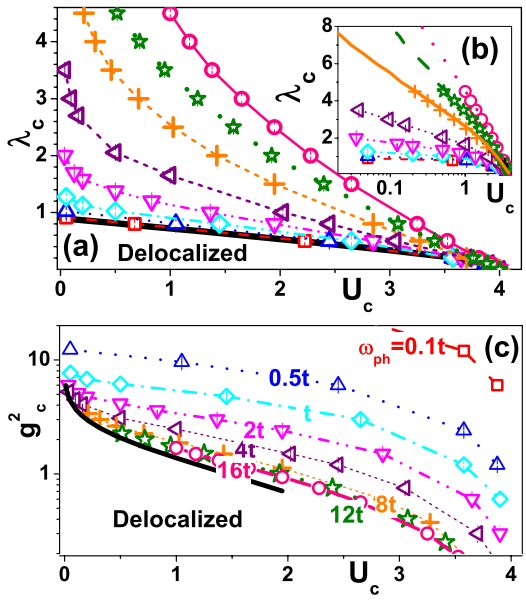

FIG. 2. (Color online) Phase boundaries between delocalized (left lower corner) and localized states of a polaron in [(a) and (b)] λ_c-U_c and (c) g_c^2-U_c coordinates: adiabatic limit $\omega_{ph}=0$ [thick solid line in panel (a)], $\omega_{ph}=0.1$ (squares), 0.5 (triangles up), 1 (diamonds), 2 (triangles down), 4 (triangles left), 8 (crosses), 12 (stars), 16 (circles). The thick solid curve in panel (c) is obtained from Eq. (5). Solid, dashed, and dotted lines in panel (b) are results obtained by the CBS method (Ref. 17) for $\omega_{ph}=8$, 12, and 16. The values of λ_c are set exactly, while the error bars of the quantity U_c are less than 3.0×10^{-2}.

2(b)], we see how for finite ω_{ph} our solution differs from the adiabatic result [thick solid curve in (a)]. With g_c^2-U_c coordinates ($g=\gamma/\omega_{ph}$) we show the deviation from the limiting phase boundary,

$$U_c(\omega_{ph}=\infty)=U_c(\gamma=0)\exp(-g_c^2), \tag{5}$$

$\omega_{ph}\to\infty$ thick solid curve in [Fig. 2(c)]. This relation is obtained by Lang-Firsov transformation, which renormalizes hopping, and accordingly the critical U_c, as $t\mapsto t\exp(-g^2)$. An exponential relation between U_c and g_c^2 (or $\lambda_c=g_c^2\omega_{ph}/6t$) is a characteristic property of the small $U_c\ll1$ and large $\lambda>1$ regimes [Fig. 2(b)] since, for large ω_{ph},

$$\lambda_c(U_c,\omega_{ph})\simeq(\omega_{ph}/6t)\ln[U_c(\gamma=0)/U_c]+\text{const}. \tag{6}$$

It is indeed seen in Fig. 2(b) that the slope of the phase boundary increases with ω_{ph}.

We note the agreement of our approach with the adiabatic limit[10] and antiadiabatic limit Eq. (5) results, as well as with the data obtained by the coherent basis states (CBS) method[17] for small U. Another proof of validity comes from the verification of our direct-space DMC data against those from momentum space DMC method (Fig. 6 in Ref. 18), when the "impurity" is modeled as an exciton-polaron with heavy hole and light electron.

Let us finally discuss two essential features of the phase diagram, which are entirely missing in the AA. The first is realized at large el-ph couplings where the polarons are already self-trapped but not yet confined by shallow impurities [cross-hatched region in Fig. 3(a)]. The self-trapping coupling λ_{ST}, locating the crossover from the weak- to strong-coupling regime, can be defined, e.g., as the maximum of the derivative of the average number of phonons in the ground state $N_{av}=\langle b^\dagger_{\mathbf{q}=\mathbf{0}}b_{\mathbf{q}=\mathbf{0}}\rangle$ with respect to the coupling constant λ [Figs 3(b) and 3(c)]. For small enough $U\ll1$, and any given ω_{ph}, one finds a sector in the phase diagram [Fig. 3(a)] where $\lambda_{ST}(\omega_{ph})<\lambda<\lambda_c(U,\omega_{ph})$. This defines the phase of self-trapped deconfined polarons. This phase exists even for very small (finite) phonon frequencies but appears not in AA. Therefore the disagreement between approximation-free and adiabatic results is strong throughout the whole phase diagram. Starting from $\omega_{ph}/W_B>2t/12t=1/6$ in Fig. 2, the AA

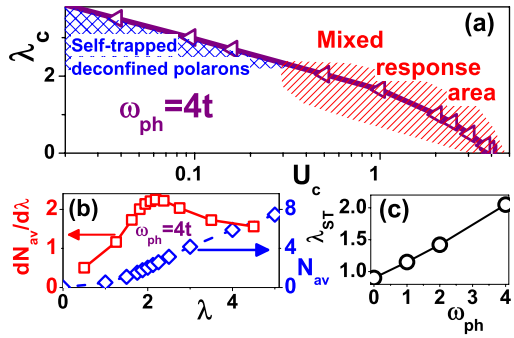

FIG. 3. (Color online) (a) Phase diagram and (b) average number of phonons N_{av} and derivative $dN_{av}/d\lambda$ for $\omega_{ph}=4$. (c) Dependence of the self-trapping coupling λ_{ST} on the phonon frequency ω_{ph} (error bars smaller than point size).

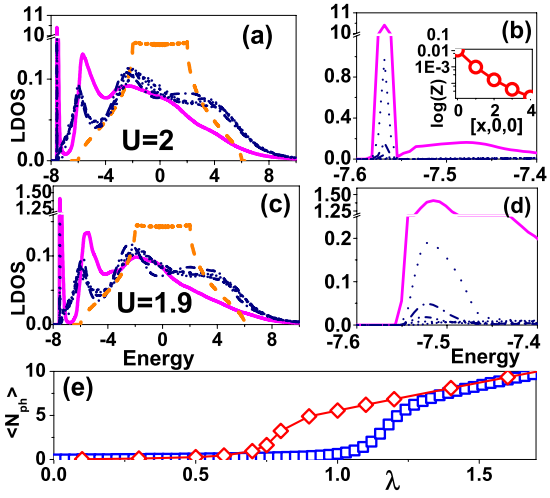

FIG. 4. (Color online) LDOS for a [(a) and (b)] localized polaron at $U=2$ and a [(c) and (d)] delocalized polaron at $U=1.9$, where $\lambda=0.8$ and $\omega_{ph}=2$. Shown is the LDOS at the impurity site (0,0,0) (solid line), nearest-neighbor site (1,0,0) (dots), site (2,0,0) (dash-dots), (3,0,0) (dash-dot-dots), (4,0,0) (short dashes), and for infinite distance from the impurity (short dots). The dashed line is the unperturbed LDOS ($\lambda=0$, $U=0$). The inset in panel (b) gives the Z factor of the LDOS δ peak of the bound state as a function of the distance to the impurity. Panel (e) shows the average number of phonons at (diamonds) and far from the impurity (squares) for $\omega_{ph}=1$ and $U=1.4$.

is obviously invalid for high-T_c superconductors where[6] the ratio of the relevant phonon energy ($\omega_{\mathrm{ph}}=70$ meV) to the bandwidth of the electronic excitation ($W_B=0.3$ eV) is roughly 1/4.

The second feature appears at moderate values of U close to the transition region between localized and extended states [line-shaded area in Fig. 3(a)]. There, the spectral properties of a polaron are strongly position dependent. In Fig. 4 we show the LDOS calculated at and in the vicinity of the impurity. Both for [(a) and (b)] localized and [(c) and (d)] extended polarons the LDOS at the impurity site strongly differs from that at the nearest-neighbor site in the [(b) and (d)] low-energy region. On the contrary, the overall features of the LDOS at the nearest-neighbor site are very similar to those at infinite distance from the defect [Figs. 4(a) and 4(c)]. This property points out how strongly the spectral properties depend on the value of the impurity potential at a given lattice site. Comparison of the average number of phonons at the impurity with that in infinite distance to the impurity [Fig. 4(e)] shows that for a wide range of parameters the lattice is weakly distorted far from the impurity while it is strongly deformed near the impurity. This demonstrates how impurities enhance the formation of small polarons.

As a consequence it is expected that in a material with imperfections a mixture of behavior typical for weak-coupling polarons (far away from an impurity) and strong-coupling polarons (close to or at the impurity) occurs. Even though the impurity concentration can be small, the induced changes, e.g., in the spectral response, can be drastic. For example, for $U=1.90$ and $\lambda=0.8$ [Fig. 1(a)] the charge density on the impurity site is four orders of magnitude larger than in the bulk of the system. Therefore, even a small impurity concentration $n_i \approx 10^{-3}$ suffices to entirely change the spectral properties. For example, since photoemission[19] and optical conductivity[20] spectra are very different for weak and strong couplings, one can expect a mixture of the spectral responses.

In conclusion, introducing the direct-space diagrammatic Monte Carlo in the thermodynamic limit, we presented the numerically exact phase diagram for localization of a polaron at an attractive impurity for all coupling strengths, values of the impurity potential, and phonon frequencies ranging from the adiabatic to the antiadiabatic regime. Most notably we characterize a phase where heavy polarons are mobile in the presence of shallow impurities and predict complex spectral properties of the systems close to the localization-delocalization transition. The present DMC method can be easily generalized to study more general situations, e.g., systems with long-range particle hopping, impurities with long-range attractive/repulsive potentials, lattice impurities, or interfaces and layered structures, demonstrating its potential for future research.

A.S.M. was supported by RFBR (Grant No. 07-02-00067a), N.N. by Grant-in-Aids (Grants No. 15104006, No. 16076205, No. 17105002, and No. 19048015) and NAREGI Japan, while A.A. and H.F. acknowledge support by DFG (Grant No. SFB 652).

[1] O. Gunnarsson, M. Calandra, and J. E. Han, Rev. Mod. Phys. **75**, 1085 (2003).
[2] S. M. Girvin and M. Jonson, Phys. Rev. B **22**, 3583 (1980); M. H. Cohen, E. N. Economou, and C. M. Soukoulis, Phys. Rev. Lett. **51**, 1202 (1983).
[3] F. X. Bronold, A. Alvermann, and H. Fehske, Philos. Mag. **84**, 673 (2004); A. Alvermann and H. Fehske, Phys. Rev. B **77**, 045125 (2008).
[4] J. P. Hague, P. E. Kornilovitch, and A. S. Alexandrov, Phys. Rev. B **78**, 092302 (2008).
[5] P. A. Lee, N. Nagaosa, and X.-G. Wen, Rev. Mod. Phys. **78**, 17 (2006).
[6] O. Gunnarsson and O. Rösch, J. Phys.: Condens. Matter **20**, 043201 (2008).
[7] V. Cataudella, G. De Filippis, A. S. Mishchenko, and N. Nagaosa, Phys. Rev. Lett. **99**, 226402 (2007); A. S. Mishchenko, N. Nagaosa, Z. X. Shen, G. De Filippis, V. Cataudella, T. P. Devereaux, C. Bernhard, K. W. Kim, and J. Zaanen, *ibid.* **100**, 166401 (2008).
[8] A. J. Millis, Phys. Rev. B **53**, 8434 (1996); V. Perebeinos and P. B. Allen, Phys. Rev. Lett. **85**, 5178 (2000); A. Weiße and H. Fehske, New J. Phys. **6**, 158 (2004).
[9] G. F. Koster and J. C. Slater, Phys. Rev. **96**, 1208 (1954).
[10] Y. Shinozuka and Y. Toyozawa, J. Phys. Soc. Jpn. **46**, 505 (1979).
[11] A. S. Mishchenko, N. Nagaosa, N. V. Prokofev, A. Sakamoto, and B. V. Svistunov, Phys. Rev. B **66**, 020301(R) (2002); A. Alvermann, H. Fehske, and S. A. Trugman, *ibid.* **78**, 165106 (2008).
[12] A. S. Mishchenko, N. V. Prokof'ev, A. Sakamoto, and B. V. Svistunov, Phys. Rev. B **62**, 6317 (2000); A. S. Mishchenko, Phys. Usp. **48**, 887 (2005); A. S. Mishchenko and N. Nagaosa, J. Phys. Soc. Jpn. **75**, 011003 (2006).
[13] K. Vafayi and O. Gunnarsson, Phys. Rev. B **76**, 035115 (2007).
[14] A. Macridin, G. A. Sawatzky, and M. Jarrell, Phys. Rev. B **69**, 245111 (2004).
[15] P. E. Kornilovitch, Phys. Rev. Lett. **81**, 5382 (1998).
[16] L.-C. Ku and S. A. Trugman, Phys. Rev. B **75**, 014307 (2007).
[17] V. Cataudella, G. De Filippis, F. Martone, and C. A. Perroni, Phys. Rev. B **70**, 193105 (2004); G. De Filippis, V. Cataudella, V. Marigliano Ramaglia, and C. A. Perroni, *ibid.* **72**, 014307 (2005).
[18] E. Burovski, H. Fehske, and A. S. Mishchenko, Phys. Rev. Lett. **101**, 116403 (2008).
[19] A. S. Mishchenko and N. Nagaosa, Phys. Rev. Lett. **93**, 036402 (2004).
[20] A. S. Mishchenko, N. Nagaosa, N. V. Prokof'ev, A. Sakamoto, and B. V. Svistunov, Phys. Rev. Lett. **91**, 236401 (2003); G. De Filippis, V. Cataudella, A. S. Mishchenko, C. A. Perroni, and J. T. Devreese, *ibid.* **96**, 136405 (2006).